Colloids and Surfaces B: Biointerfaces 245 (2025) 114221

Contents lists available at ScienceDirect

Colloids and Surfaces B: Biointerfaces

journal homepage: www.elsevier.com/locate/colsurfb

# Utilization of chitosan nanocomposites loaded with quantum dots enables efficient and traceable DNA delivery

Jiayu He [a], Peng Hu [a], Mingjie Wang [a], Guowei Qi [a], Haoxiang Huang [a], Dong Zeng [a], Jintao Guan [b], Peiwen Lv [b], Liang Liu [a,*]

[a] School of Life Science and Technology, Wuhan Polytechnic University, Wuhan 430023, China
[b] School of Chemical and Environmental Engineering, Wuhan Polytechnic University, Wuhan 430023, China

ARTICLE INFO

*Keywords:*
DNA delivery
Chitosan
Quantum dots
Gene carriers

ABSTRACT

Chitosan is widely employed in gene carriers due to its excellent gene loading capacity, ease of modification, and exceptional biodegradability. However, low gene delivery efficiency, high cytotoxicity, and lack of tracer biomimetic properties limit its clinical use. To address these issues, a novel biomimetic tracking gene delivery carrier, RBCm-C50kQT, was constructed by using the design scheme of cell membrane coated carbon quantum dots/chitosan. This carrier improves stability and tracking performance while embedding the cell membrane enhances biosafety. RBCm-C50kQT effectively carries and protects DNA, improving uptake and transfection efficiency with reduced cytotoxicity. It maintains strong fluorescence tracking and shows high uptake efficiencies of 83.62 % and 77.45 % in 293 T and HeLa cells, respectively, with maximum transfection efficiencies of 68.80 % and 45.47 %. This advancement supports gene therapy improvements and paves the way for future clinical applications.

## 1. Introduction

Gene therapy holds immense promise but encounters hurdles like delivery technology limitations and biosafety concerns [1]. Cationic polymers such as chitosan (CS), poly-L-lysine (PLL), and polyethyleneimine (PEI) dendrimers are favored for their lower immunogenicity and improved safety, addressing these issues effectively [2,3]. CS, a natural polysaccharide cationic polymer, features abundant positive charges that facilitate electrostatic interactions with DNA, aiding in nucleic acid protection and condensation [4,5]. Its low toxicity, good biodegradability, and modifiable nature make it ideal for advanced therapeutic and diagnostic applications, including cancer diagnosis, imaging and treatment [6,7]. Especially, CS has become one of the most extensively researched gene carriers due to its efficient gene expression and excellent biocompatibility [8,9]. To observe the biological imaging process of chitosan, it is often coupled with organic dyes, fluorescent proteins, and other fluorescent groups to give it optical (fluorescent) properties [10–12]. However, traditional fluorescent labeling methods suffer from poor photostability, low hydrophilicity, and high toxicity, limiting their application in gene delivery [13–15]. To solve this issue, it is urgent to prepare a gene delivery carrier with high fluorescence intensity and good stability. Quantum dots have become the focus of attention because of their excellent optical properties and good biocompatibility.

Quantum dots (QDs) have been widely studied due to their unique properties such as high photostability, high biocompatibility, wide excitation and photoluminescence [16–18]. The superior fluorescence properties, which can be excited and visualized in physical environments and make QDs ideal for applications in cell imaging, biofluorescent labeling, and related fields [19–21]. However, small quantum dots are easily endocytosed by cells and degraded by nucleases [22]. When a single quantum dot is used as a gene carrier, its ability to carry DNA is limited [23]. To address this issue, researchers have developed quantum dots with various surface chemical modifications as probes for *in vitro* and *in vivo* imaging, and multifunctional quantum dot carriers for precise gene delivery, integrated diagnosis and treatment [24–27]. Lee et al. created carboxymethyl chitosan-coated zinc oxide QDs, enhancing stability and improving release, imaging, and therapeutic outcomes [28]. Similarly, Santanu Ghosh's team synthesized carbon QDs conjugated with polyamidoamine (PAMAM) dendrimers for gene delivery, showing potential in breast cancer detection and therapy [29]. Despite their promise, challenges such as low gene delivery

* Corresponding author.
*E-mail address:* hustll@126.com (L. Liu).

https://doi.org/10.1016/j.colsurfb.2024.114221
Received 18 June 2024; Received in revised form 27 August 2024; Accepted 8 September 2024
Available online 10 September 2024

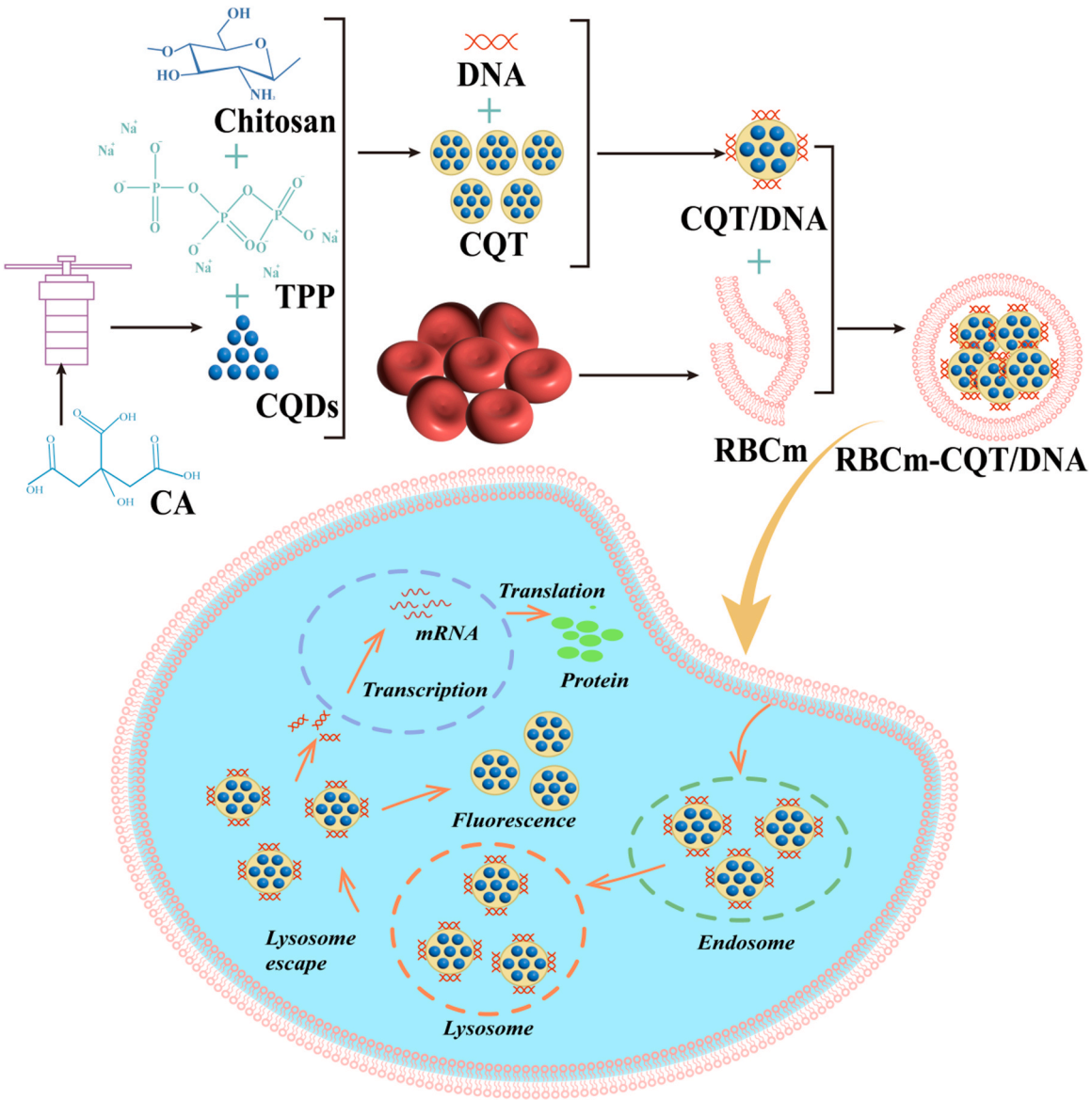


**Scheme1.** The preparation scheme of CS-CQDs- TPP/DNA and RBCm-CQT/DNA complexes, as well as the transport and gene transfection of the complexes in cells.

efficiency and high cytotoxicity remain significant in clinical applications [30–32].

In recent years, cell membrane has been widely used in the embedding of gene carriers because of its good biocompatibility and biodegradability [33,34]. Encapsulation with cell membranes enhances carrier particle stability and biosafety by mitigating environmental influences [35–37]. Red blood cells are the most abundant circulating cells in blood, with good biocompatibility, degradability and long half-life [38,39]. Nanoparticles coated with erythrocyte membranes benefit from prolonged *in vivo* retention and increased tumor targeting [40,41]. Therefore, erythrocyte membranes were widely used in drug delivery systems and gene delivery systems. Wang et al. encapsulated PEI/DNA complexes within erythrocyte membranes, creating the RBCm-PDc complex with low protein adsorption, reduced cytotoxicity, and high gene delivery efficiency [42]. Liang et al. developed RP-PU by embedding probuol (PU) in erythrocyte membranes, demonstrating sustained release, good biocompatibility, and effective cellular internalization [43]. These advancements highlight the potential of membrane-encapsulated gene delivery systems for effective gene therapy. However, most of the reports focused on the transfection efficiency and cytotoxicity, and there were still few reports on visual gene vectors with good biocompatibility, low toxicity and fluorescence characteristics.

In this work, we constructed a tracking biomimetic gene delivery vector based on cell membrane encapsulated carbon quantum dots/chitosan (RBCm-C50kQT) to achieve safe and effective gene delivery. As demonstrated in Scheme 1, biosafety carbon quantum dots were prepared by a simple hydrothermal method using citric acid (CA) as raw material. Subsequently, TPP was attached to chitosan (Chitosan30k and Chitosan50k) to functionalize the surface of CQDS to enhance DNA binding while preserving the biological tracking properties of the quantum dots. Finally, the natural cell membrane was embedded to further improve its stability and biosafety. The biological tracking characteristics of the carrier material were verified by fluorescence emission spectrum, the surface morphology of the carrier was observed by scanning electron microscope and transmission electron microscope, the biological safety of the carrier was verified by MTT assay, and its effectiveness as a gene carrier was detected by agarose gel electrophoresis, *in vitro* cell uptake experiment and *in vitro* cell transfer staining, indicating that it is a safe and effective gene carrier.

## 2. Experimental section

### 2.1. Preparation of CQDs and CS-CQDs-TPP

After dissolving 3.84 g CA in 20 mL purified water, it was transferred into a high-pressure stainless steel reactor lined with polytetrafluoroethylene and yellow liquid was obtained after reaction at 200 ℃ for 3 h. And subsequently dialyzed in the dark for 24 h. The resulting dialysate was freeze-dried to obtain CQDs powder.

After 10 mg Chitosan50k was ultrasonically dissolved in 5 mL 5 % acetic acid to obtain 2 mg/mL Chitosan50k storage solution. A certain amount of storage solution was weighed into a clean beaker, and the mixture of CQDs and TPP was slowly added while stirring, and the reaction was continued for 2 h at room temperature. After the reaction was completed, Chitosan50k-CQDs-TPP (C50kQT) was obtained by centrifuge at 12,000 rpm/min for 30 min, precipitation was removed, and freeze-drying was performed. Using the same method, Chitosan30k is substituted for Chitosan50k to obtain Chitosan30k-CQDs-TPP (C30kQT).

### 2.2. Preparation of CS-CQDs-TPP/DNA , RBCm-CQT/DNA

The C30kQT/DNA complex was prepared by mixing C30kQT and DNA according to a certain mass ratio and incubating for 60 min. The prepared RBCm suspension was thawed and dispersed ultrasonic, mixed according to the mass ratio of RBCm to C30kQT/DNA complex of 0.5/1.5/1, 1/1.5/1, 2/1.5/1, 3/1.5/1, 4/1.5/1, and incubated at room temperature for 1 h after 60 s of vortex. After incubation, Genizer liposome extruder was used to prepare compounds with different mass ratios. The preparation method of C50kQT/DNA and RBCm-C50kQT/DNA complex is the same as above.

### 2.3. Characterization of CS-CQDs-TPP/DNA , RBCm-CQT/DNA

#### 2.3.1. Fluorescence characterization

Quantum dots can deliver genes because of their unique optical properties, and can visualize the gene delivery process in real time. To validate the fluorescence properties of C30kQT and C50kQT, they were dispersed in deionized water, and the fluorescence emission spectra of C30kQT and C50kQT were measured using a fluorescence microplate reader (EnSpireTM, PerkinElmer, US) at different excitation wavelengths.

#### 2.3.2. Fourier transform infrared spectroscopy (FTIR)

The surface functional groups of CA, CQDs, Chitosan30k, Chitosan50k, C30kQT and C50kQT were identified using FTIR. The samples were mixed with potassium bromide at a mass ratio of 1/100, and then ground into thin transparent discs. The infrared spectrum was documented after measuring the infrared absorption in the range of 400–4000 $cm^{-1}$ using an infrared spectrometer (INVENIO, BRUKER, GER).

#### 2.3.3. Determination of amino group content

20 μL of a fluorescent amine solution (1 mg/mL) and 2 μL of C30kQT (1 mg/mL) solution were added to 100 μL of deionized water and incubated at room temperature for 10 min. The fluorescence intensity of the mixture was measured by 3D fluorescence scanning with the excitation wavelength range of 320–410 nm and the emission wavelength range of 450–600 nm, and the 3D fluorescence map was drawn. And then the standard curve was constructed according to the amino group content and fluorescence intensity in Chitosan50k. The content of amine group in the sample was calculated according to formula (1). Where $F_1$ is the final concentration of the sample mixed with fluorescent amine, and $F_0$ is the theoretical concentration obtained by substituting the fluorescence value data of the test group into the standard curve.

$$\text{Amine group content} = \frac{F_1}{F_0} \times 6.2 \times 10^{-5} \quad (1)$$

#### 2.3.4. Size and zeta potential

The dynamic light scattering (DLS) technique was employed to assess the particle size and potential of C30kQT and C50kQT nanocomposites. Purified water (Hangzhou Wahaha Group Co., LTD.) was used to resuspend the pellets containing the particles. Then the particle size and zeta potential of the nanocomposites were measured using a Zetasizer Nano ZS (Marvin, UK) at 25 °C. The average value was calculated based on the results of three measurements, with a standard deviation of ± SD. The particle size and zeta potential determination methods of RBCm-C30kQT/DNA and RBCm-C50kQT/DNA complexes are the same as above.

#### 2.3.5. SEM and TEM

The morphology of C30kQT, C50kQT, RBCm-C30kQT/DNA and RBCm-C50kQT/DNA were characterized by SEM (FSEM-1, Sirion 200, NED) and TEM (FEI Talos F200X G2, USA). 30 μL of the solution was dropped onto the wafer, drying at room temperature and then under field emission scanning electronmicro scop detection for SEM images. The nanoparticles were dispersed with deionized water, and 50 μL of the solution was added dropwise onto a copper mesh, which was allowed to dry at room temperature, and then the morphology and size of the nanoparticles were observed by TEM.

### 2.4. Hemolysis test

10–20 mL of fresh mouse whole blood (which had been added with anticoagulant Active Ingredient sodium) was added to the test tube and diluted with proper amount of normal saline. Centrifuge was centrifuged at 2000 rpm/min and precipitation was left, and then washed with normal saline repeatedly for 2–3 times to prepare a normal saline suspension with 2 % concentration. Chitosan30k, Chitosan50k, C30kQT and C50kQT were mixed with 1 mL 2 % red blood cell suspension, 10 % Triton X-100 was the positive control group, and the normal saline group was the negative control group. The prepared sample was then incubated at 37 ℃ for 1 h, centrifuged at 2000 rpm/min and then su-pernatant was taken to determine its maximum UV absorption at 418 nm. The samples in each group were measured three times in par-allel, and the hemolysis rate was calculated according to formula (2). Where A is the absorbance of the experimental group, $A_T$ is the absor-bance of the positive control 10 % Triton X-100 group, and $A_0$ is the absorbance of the negative control normal saline group.

$$\text{Hemolysis rate} = \frac{A - A_0}{A_T - A_0} \times 100\% \quad (2)$$

### 2.5. Agarose gel electrophoresis

Agarose gel electrophoresis was used to assess the DNA condensation ability of C30kQT and C50kQT. After the carrier/DNA complexes with various mass ratios were added to the 1 % (w/v) agarose gel sample wells containing EtBr, the gel was placed in TBE buffer and subjected to electrophoresis at 90 V for 40 min. Finally, the gel imaging system was utilized to observe the gel image.

In the DNA protection and release evaluation experiment, three groups of C30kQT/DNA, C50kQT/DNA and Chitosan50k/DNA complexes were prepared according to the optimal binding mass ratio, and the band changes of agarose gel electrophoresis were observed after different treatments. The treatment methods for each experimental group are as follows: Group I serves as the negative control without any treatment, with well 0 as the DNA blank control; Group II includes the addition of 4 μL of Active Ingredient sodium (20 mg/mL); Group III involves the addition of 3 μL of DNaseI (40 U/mL) and 3 μL of Reaction Buffer (10×);

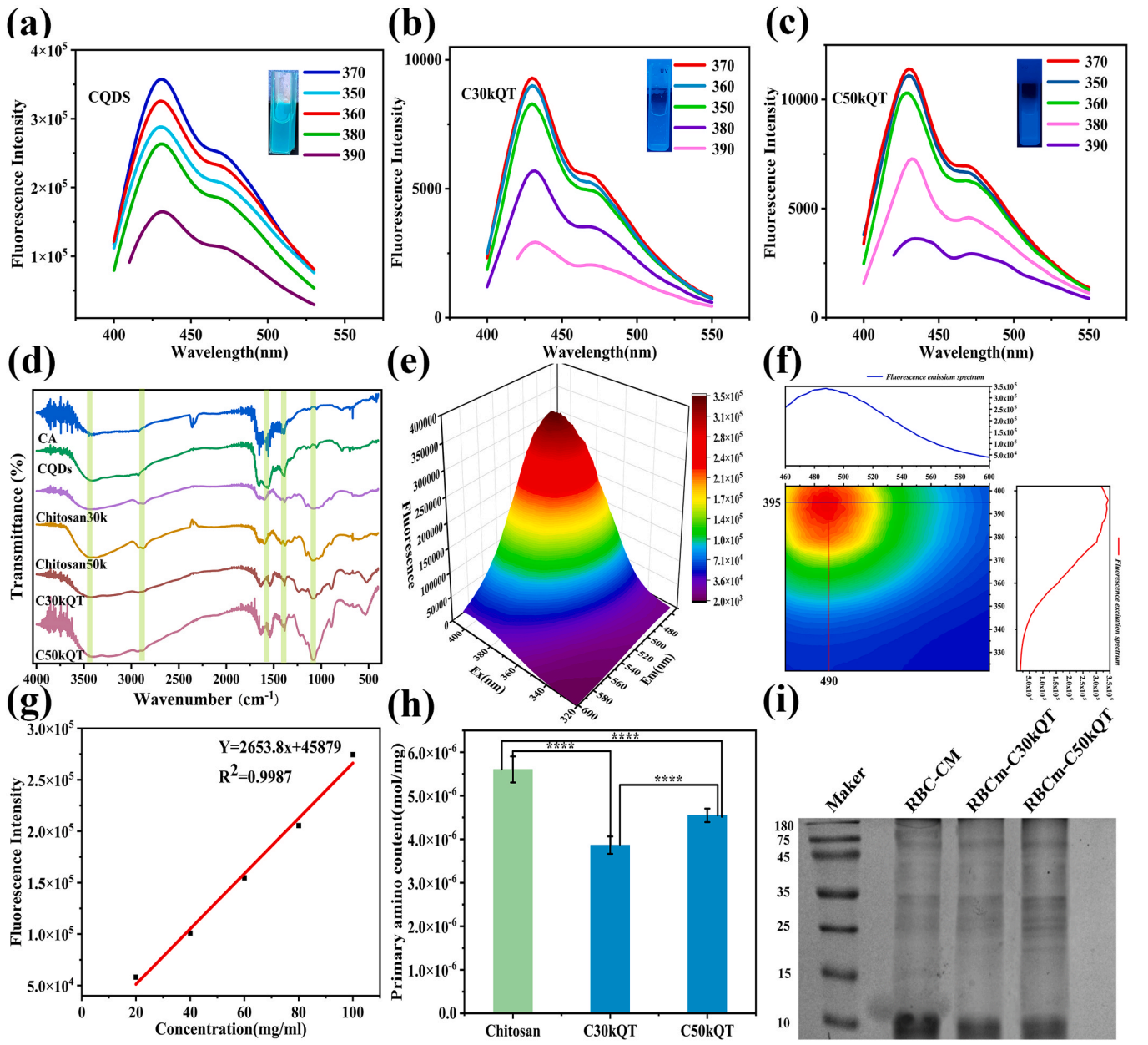


**Fig. 1.** Characterization results. (a), (b), (c) Fluorescence emission spectra of CQDs, C30kQT and C50kQT at different excitation wavelength. (d) FTIR spectra of CA, CQDs, Chitosan30k, Chitosan50k, C30kQT and C50kQT. (e) 3D fluorescence map of fluorescent amine derivatives. (f) Fluorescent amine derivative contour fluorescence map. (g) Amino content standard fluorescence curve. (h) Amino group content of C30kQT and C50kQT. (mean ± SD, n = 3; $*p \leq 0.05$, $**p \leq 0.01$, $***p \leq 0.001$, $****p \leq 0.0001$). (i) SDS-PAGE electrophoretic analysis of the film coated complex.

Group IV starts with the addition of 4 μL of Active Ingredient sodium (20 mg/mL) followed by 3 μL of DNaseI (40 U/mL) and 3 μL of Reaction Buffer (10×); Group V begins with the addition of 3 μL of DNaseI (40 U/mL) and 3 μL of Reaction Buffer (10×) followed by 2.5 μL of EDTA (50 mM) and 4 μL of Active Ingredient sodium (20 mg/mL).

### 2.6. SDS-PAGE

The effectiveness of cell membrane encapsulation was assessed using SDS-PAGE. The gel was prepared following the instructions provided in the kit. A mixture of 10 μL of sample buffer (5×) and 40 μL of carrier nanocomposites (1 mg/mL) was boiled in a water bath for 10 min. After centrifugation at 3000 rpm for 1 min, the supernatant was loaded into the gel. Electrophoresis was then run at 80 V for 30 min, followed by electrophoresis at 120 V for 2 h until the bromophenol blue dye reached the bottom of the gel. The gel was stained with G250 for 1 h and then decolorized using a decolorizing solution. Finally, the gel image was observed using a gel imaging system (Gel Doc XR, Bio-Rad, US).

### 2.7. MTT assay

MTT method was used to determine the effect of samples on cell growth status, and the relative cell survival rate was used as the final evaluation basis. The cells were seeded in a 96 well plate at a density of 1 × $10^4$ cell/well and then incubated for 24 h until they reached 80 % confluence. After the culture medium was replaced, a complete culture medium containing different concentrations of carrier or carrier/DNA nanocomposites was added. Following a 48 h incubation and 72 h incubation, 100 μL of MTT (0.5 mg/mL) solution was added to each well, and the cells were then incubated for 4 h. Subsequently, the purple

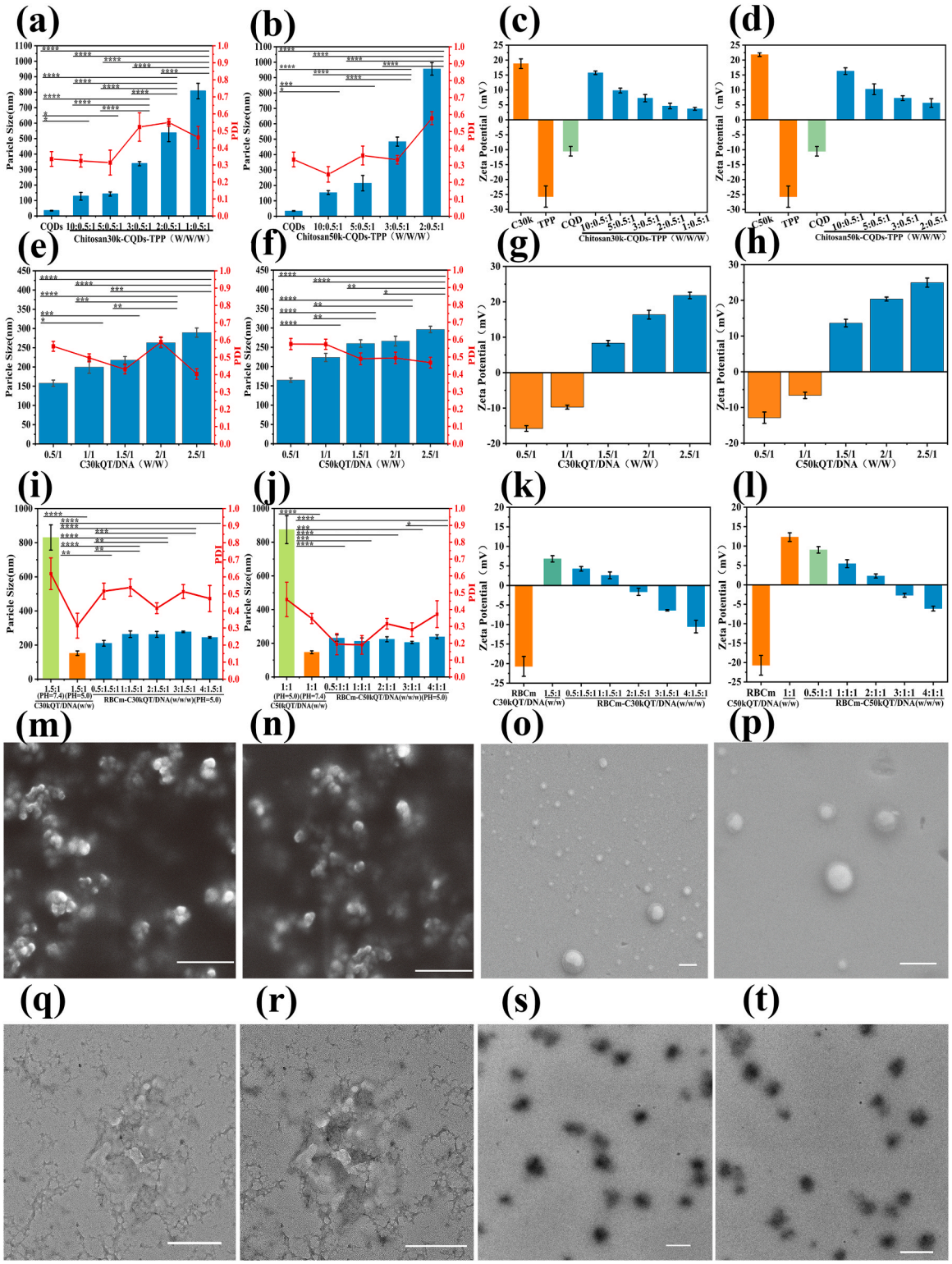


**Fig. 2.** Characterization results. (a-d) Particle size and potential of Chitosan/CQDs/TPP with different mass ratios. (e-h) Particle size and potential of Chitosan/CQDs/TPP/DNA with different mass ratios. (i-l) Particle size and potential of RBCm-CQT/DNA with different membrane mass ratios. (mean ± SD, n = 3; $^{*}p \leq 0.05$, $^{**}p \leq 0.01$, $^{***}p \leq 0.001$, $^{****}p \leq 0.0001$). (m-p) Scanning electron microscope images of C30kQT, C50kQT, RBCm-C30kQT and RBCm-C50kQT. (Scale ratio = 500 nm.) (q-t) Transmission electron microscopy images of C30kQT, C50kQT, RBCm-C30kQT and RBCm-C50kQT. (Scale ratio = 500 nm.).

methylzan crystal was dissolved by adding an equal amount of DMSO, and the absorbance of each well at 570 nm was then measured using a microplate reader (EnSpire™, PerkinElmer, US). The relative cell survival rate was calculated by formula (3), and 3 parallel sets were set for each sample. The average value of the obtained data was used to calculate the relative cell survival rate, and the standard deviation was ±SD. Where $A_0$ is the absorbance per hole of the experimental group, and $A_{570}$ is the absorbance of the negative control group.

$$\text{Cell viability} = \frac{A_0}{A_{570}} \times 100\% \quad (3)$$

### 2.8. In vitro cell uptake

Ensuring that carriers have efficient cellular uptake is a key factor for successful gene delivery. The uptake efficiency of C30kQT/DNA, C50kQT/DNA, RBCm-C30kQT/DNA and RBCm-C50kQT/DNA nanocomposites was investigated in 293 T and HeLa cells. The cells were seeded in a 12-well plate and incubated until they reached 70–80 % confluence. The culture medium was then replaced with DMEM medium containing carrier/DNA nanocomposites, with DNA mass of 2 μg/well. After the cells were cultured for an additional 6 h, they were fixed with 4 % paraformaldehyde and the culture medium was removed. The cells were then stained with Green488 dye and observed using a confocal laser scanning microscope (IRX60, Sunny Optical Technology, China). The cellular uptake efficiency of the complexes was also quantified using flow cytometry (CytoFLEX, Beckman, US).

### 2.9. In vitro gene transfection

The efficacy of gene carriers is often evaluated based on transfection efficiency, which is considered one of the most important indicators. The transfection efficiency of C30kQT/DNA, C50kQT/DNA, RBCm-C30kQT/DNA, and RBCm-C50kQT/DNA complexes was investigated in 293 T and HeLa cells. The cells were initially placed in a 24-well plate at a density of $1\times10^4$ and left to incubate for 24 h. Following this, medium containing various mass ratios of carriers/DNA complexes, with a DNA mass of 1 μg/well, was added to the cells and they were further incubated for 6 h. The culture medium was then replaced with DMEM medium containing complete medium, and the cells were left to incubate for an additional 48 h. Subsequently, the cells were washed three times with PBS, and the expression of GFP in the cells was observed using fluorescence microscopy (BA400, Motic, CN). The transfection efficiency was then quantitatively analyzed using flow cytometry.

### 2.10. Statistical analysis

The data was presented as mean ± SD, and Origin 2021 software was used for data analysis. Statistical significance was indicated by $^*p \leq 0.05$, $^{**}p \leq 0.01$, $^{***}p \leq 0.001$, $^{****}p \leq 0.0001$.

## 3. Results and discussion

### 3.1. Characterization of carriers

#### 3.1.1. Fluorescence characterization

Fig. 1**a-c** showed the fluorescence emission spectra of CQDs, C30kQT and C50kQT at different excitation wavelengths. The excitation spectrum peak pattern of CQDs conforms to the characteristics of wide excitation and narrow emission of quantum dots [44]. The fluorescence intensity first increases and then decreases, and the fluorescence emission peak intensity was the largest when excited at 370 nm. C30kQT and C50kQT have the largest fluorescence emission peak intensity when excited at 370 nm, which is similar to CQDs. The results show that C30kQT and C50kQT have similar photoluminescence properties as quantum dots, and can be used to trace gene delivery.

#### 3.1.2. Detection of characteristic photofunctional groups

To assess the successful incorporation of CQDs into chitosan-TPP coatings, FTIR spectra of various nanocomposites were analyzed using an infrared spectrophotometer ((INVENIO, BRUKER, GER). As shown in Fig. 1**d**, the FTIR spectrum of chitosan exhibits peaks at 3430 $cm^{-1}$ for hydroxyl and amino stretching vibrations, as well as at 2864 $cm^{-1}$ for C-H stretching [45]. Additionally, distinct characteristic peaks of chitosan repeating units (COC) at 1077 $cm^{-1}$ and 890 $cm^{-1}$ were observed, consistent with literature reports [46]. The spectra of carbon quantum dots and citric acid are alike, exhibiting prominent infrared absorption peaks at 1647 $cm^{-1}$ and 1393 $cm^{-1}$ (related to symmetric and asymmetric stretching vibrations of carbonyl groups) as well as 1560 $cm^{-1}$ (indicative of bending vibration of hydroxyl groups) [47]. When compared to individual chitosan and carbon quantum dots, the primary infrared peaks are visible in the FTIR spectrum of C30kQT and C50kQT. Notably, the absorption peak at 1077 $cm^{-1}$ exhibits a noticeable enhancement in peak width and intensity, which is a result of the superposition of the bending vibration peak of hydroxyl groups in carbon quantum dots and the characteristic peak of COC in chitosan. The above results confirm the feasibility of the synthesis strategy for C30kQT and C50kQT.

#### 3.1.3. Determination of amino group content

The amino content was closely related to the charge on the carrier and can be used as an evaluation index of the charge intensity of the carrier [48]. The fluorescence standard curve method was used to determine the amino content on the surface of the carrier. The three-dimensional fluorescence spectrum and isoline fluorescence spectrum of chitosan50k after reaction with fluorescent amine were displayed in Fig. 1**e-f**, the maximum excitation wavelength and emission wavelength were about 395 nm and 490 nm. As illustrated in Fig. 1**g**, there was a typical linear relationship between fluorescence intensity and concentration. The primary amine contents of C30kQT and C50kQT are $3.86\times10^{-6}$ mol/mg and $4.54\times10^{-6}$ mol/mg, respectively (Fig. 1**h**). The results showed that C50kQT had higher amino content and generated higher charge, which had better ability to carry DNA.

#### 3.1.4. SDS-PAGE

The surface protein profiles of RBCm-C30kQT/DNA and RBCm-C50kQT/DNA were analyzed by SDS-PAGE. As illustrated in Fig. 1**i**, the protein electrophoretic bands of RBCm-C30kQT/DNA and RBCm-C50kQT/DNA showed protein profiles with molecular weights between 10 and 180 kDa. Although the extrusion of cell membrane by liposome extruder caused some protein loss during sample preparation, most of the protein in cell membrane was still retained. It can ensure the integrity of its physiological characteristics to a certain extent, which was conducive to improving its biological safety and transfection efficiency.

#### 3.1.5. Particle size and zeta potential

The size of carrier particle size was a key factor affecting the efficiency of cell intake, and its surface charge also affects cytotoxicity [49,50]. As shown in Fig. 2**a-b**, the size of single CQDs was about 30 nm, and the polydispersity coefficient was about 0.4, which proved that it has good dispersion. The particle size of C30kQT and C50kQT was related to the proportion of chitosan in the complex. With the decrease of the proportion of Chitosan30k and Chitosan50k, the particle size of the complex also increased. When the proportion of chitosan was too low, the distribution of the complex system was uneven and easy to agglomerate, which seriously affected the intake efficiency of the carrier. At the same mass ratio, Chitosan50k has a larger particle size than Chitosan30k, due to the higher molecular weight of Chitosan50k, which can encapsulate more carbon quantum dots. The size of the nanocomposite particles composed of C30kQT and C50kQT with DNA was shown in Fig. 2**e-f**. With the increase of the ratio of C30kQT and C50kQT, the particle size increases, but it remains at about 150–300 nm. High surface charge will lead to strong cation toxicity, The Zeta potential results of C30kQT and C50kQT were shown in Fig. 2**c-d**, The surface potentials of C30k, C50k, TPP and CQD were 19 mV, 22 mV, −26 mV and −11 mV, respectively. As the proportion of chitosan added decreased, the potential of the complex showed a downward trend. The Zeta potentials of C30kQT/DNA and C50kQT/DNA were shown in Fig. 2**g-h**, as the mass ratio increases, the potentials of C30kQT and C50kQT complexes with DNA change from negative to positive. Due to

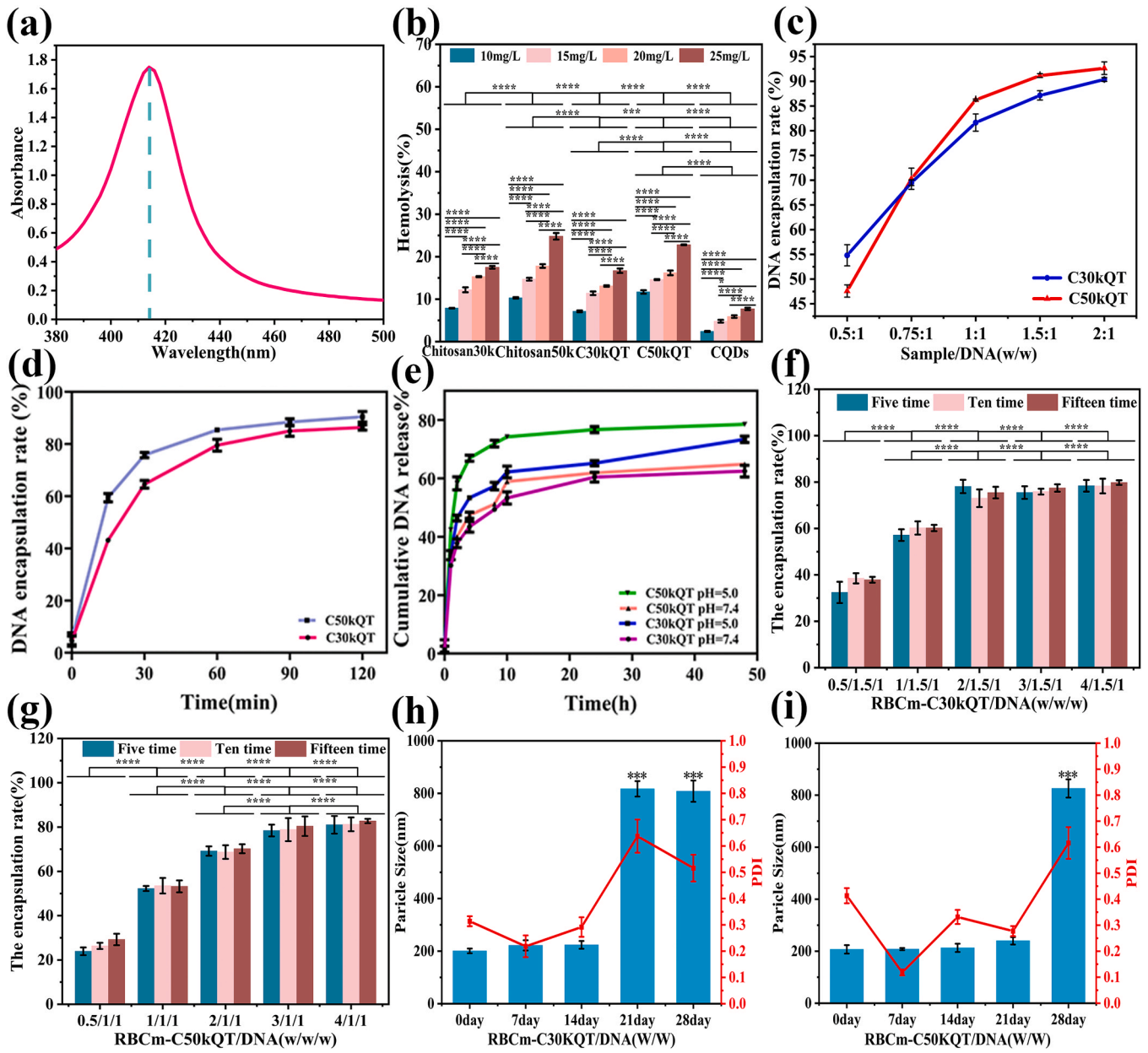


**Fig. 3.** Characterization results. (a) Red blood cell scanning at 380–500 nm ultraviolet band. (b) Hemolysis test results of C30kQT, C50kQT and CQDs at different concentrations (mean ± SD, n = 3, $^{*}p \leq 0.05$, $^{**}p \leq 0.01$, $^{***}p \leq 0.001$, $^{****}p \leq 0.0001$). (c) DNA encapsulation rate of CQT/DNA complex under different mass ratios. (mean ± SD, n = 3). (d) DNA encapsulation rate of CQT/DNA complex at different binding times. (mean ± SD, n = 3). (e) DNA release rate of C30kQT and C50kQT at pH=5.0 and pH=7.4. (f-g) The encapsulation rate of C30kQT/DNA and C30kQT/DNA complex by RBCm under different extrusion times and mass ratio (mean ± SD, n = 3, $^{*}p \leq 0.05$, $^{**}p \leq 0.01$, $^{***}p \leq 0.001$, $^{****}p \leq 0.0001$). (h) Changes in particle size of RBCmC30kQT/DNA complexes over 28 day at a mass ratio of 2/1.5/1. (mean ± SD, n = 3, $^{*}p \leq 0.05$, $^{**}p \leq 0.01$, $^{***}p \leq 0.001$, $^{****}p \leq 0.0001$). (i) Changes in particle size of RBCm-C50kQT/DNA complexes over 28 day at a mass ratio of 3/1/1. (mean ± SD, n = 3, $^{*}p \leq 0.05$, $^{**}p \leq 0.01$, $^{***}p \leq 0.001$, $^{****}p \leq 0.0001$).

the presence of positively charged amino groups on the surface of chitosan, it can neutralize the negative charge of DNA, which is beneficial for the carrier to effectively bind DNA and reduce cytotoxicity.

As displayed in Fig. 2**i-j**, when the pH changes from neutral to slightly acidic, the particle size of the carrier rapidly decreased from about 800 nm to less than 200 nm. Due to the acidic environment in tumor cells, smaller carrier particles can be better absorbed, which was conducive to the use in tumor gene therapy. The particle size of RBCm-C30QT/DNA and RBCm-C50QT/DNA was 200–300 nm, and the PDI distribution was between 0.4 and 0.6, which had good dispersion. With the increase of erythrocyte membrane mass, the total potential of RBCm-C30QT/DNA and RBCm-C50QT/DNA changed from positive to negative, which was caused by the high negative charge carried by the cell membrane (Fig. 2**k-l**). The above results illustrated that erythrocyte membrane encapsulation could reduce the excessive positive charge, which improved the biocompatibility of the carrier material.

### *3.1.6. SEM and TEM*

The SEM data results of C30kQT and C50kQT are shown in Fig. 2**m-n**. The particle size is about 100–150 nm, which was consistent with the sample size measured by DLS. The smaller size, good dispersion and uniform size made C30kQT and C50kQT more easily absorbed by cells. C30kQT and C50kQT formed a round or oval shape after being coated with cell membrane (Fig. 2**o-p**). The degree of adhesion between particles was relatively low, and the particle size basically remained at about 250 nm, with relatively uniform distribution. The results obtained

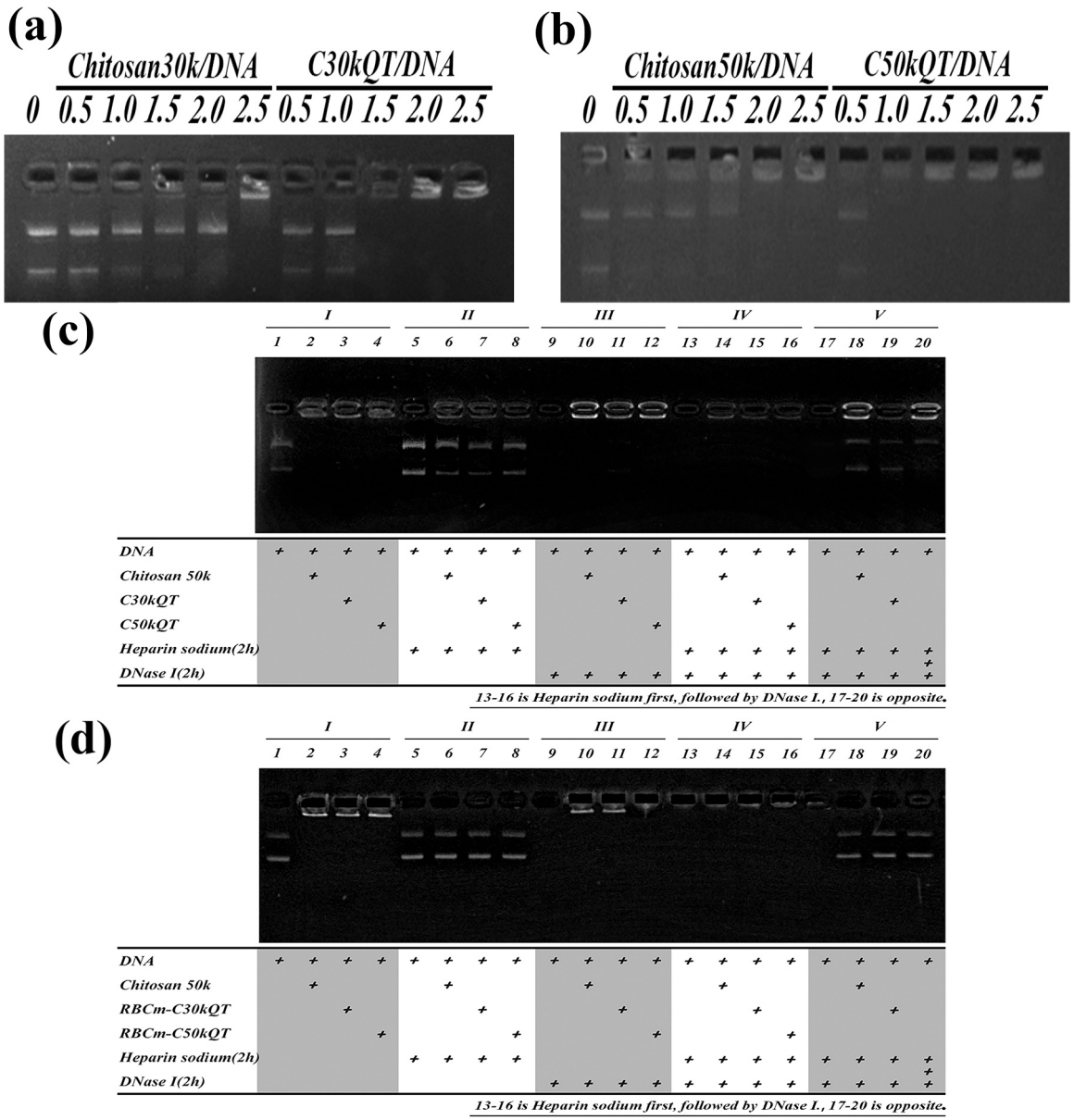


**Fig. 4.** Characterization results. (a) Results of electrophoretic migration retardations of Chitosan30k and C30kQT with DNA at different mass ratios. (b) Results of electrophoretic migration retardations of Chitosan50k and C50kQT with DNA at different mass ratios. (c) DNA protection ability of Chitosan50k/DNA, C30kQT/DNA and C50kQT/DNA complex. (d) DNA protection ability of Chitosan 50k, RBCm-C30kQT/DNA, and RBCm-C50kQT/DNA complex.

by TEM (Fig. 2**q-t**) further confirmed the successful preparation of C30kQT and C50kQT, with successful encapsulation by the cell membrane. RBCm-C30kQT and RBCm-C50kQT exhibited good dispersibility and uniform particle size. These results were highly consistent with the SEM findings, providing ample evidence that the samples were successfully prepared.

### 3.1.7. Hemolysis test

The hemolysis reaction of the C30kQT and C50kQT to red blood cells was investigated through hemolysis test. The ultraviolet absorption spectrum of red blood cell suspension in the wavelength range of 380–500 nm was shown in Fig. 3**a**, an obvious absorption peak appeared at 413 nm. Fig. 3**b** showed the hemolysis test results of C30kQT and C50kQT before and after coating, and Chitosan30k and Chitosan50k were used as positive controls. The hemolysis rate of each group gradually increased with the increase of concentration. At the same concentration, the hemolysis rates of all samples were as follows: Chitosan50k> C50kQT> Chitosan30k> C30kQT> CQDs. The results showed that the addition of CQDs could contribute to reduce the hemolysis rate of the carrier, thus effectively reducing cytotoxicity and improving biocompatibility.

### 3.1.8. Encapsulation rate and release rate

Researching and analyzing the fluorescence intensity of DAPI-DNA in the supernatant, the binding efficiency of the carrier /DNA were obtained. As shown in Fig. 3**c**, the optimal binding rate of C30kQT/DNA reached 86.24 % when the mass ratio was 1.5/1, and the optimal binding rate of C50kQT/DNA reached 87.15 % at a mass ratio of 1/1, demonstrating that C30kQT and C50kQT have better ability to bind DNA. As shown in Fig. 3**d**, the binding rates of C30kQT and C50kQT to DNA increased with time, reaching the maximum at 60 min. At this time, the binding rates of C30kQT and C50kQT to DNA were 79.55 % and 85.43 %, respectively. DNA release experiments were conducted to investigate the stability and release efficiency of the carrier, and the experimental results were shown in Fig. 3**e**. The release efficiency of C50kQT and C30kQT at pH = 5.0 were significantly higher than that at

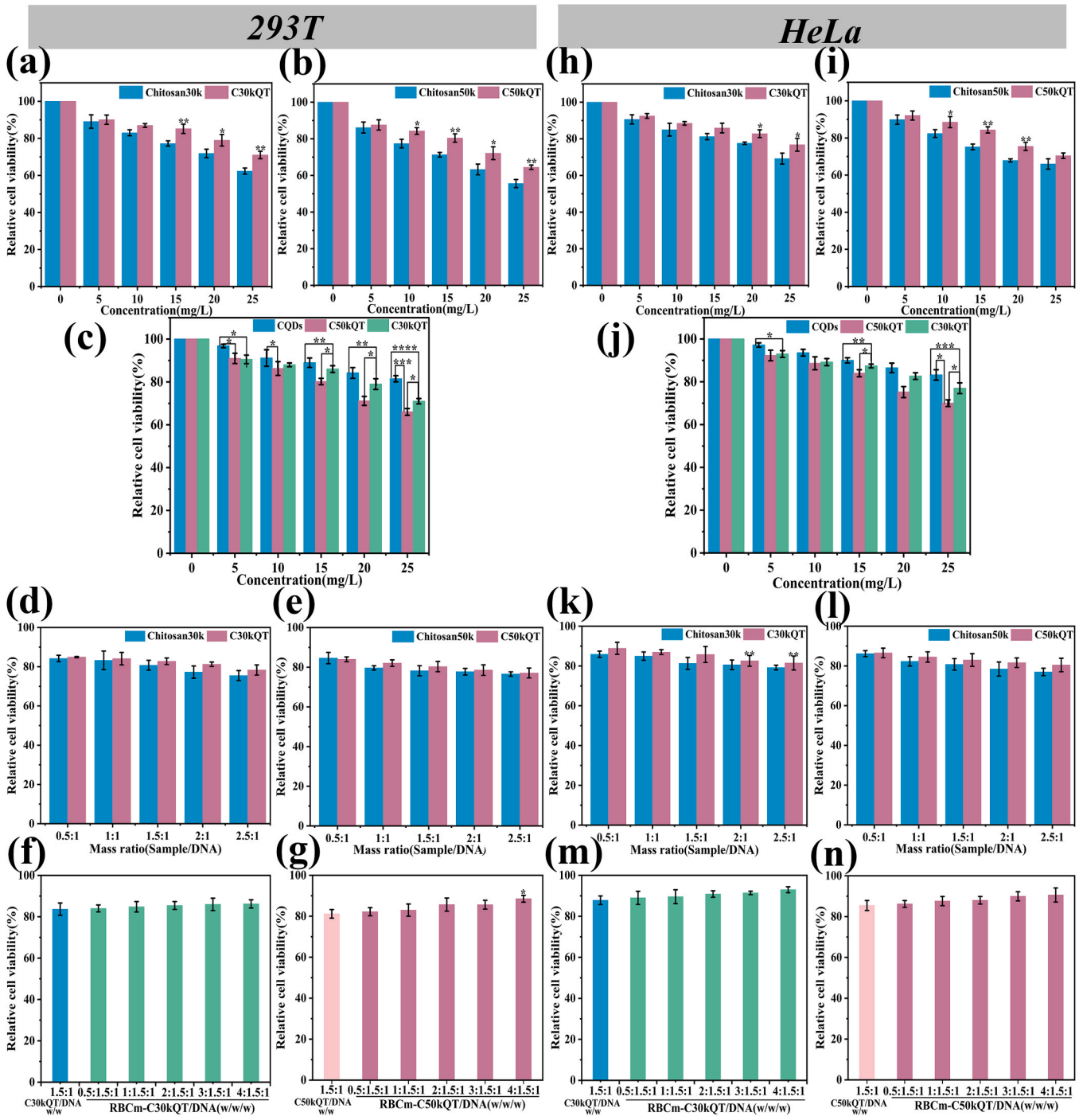


**Fig. 5.** MTT assay results (48 h incubation). (a-c) 293 T cells viability after treated by C30kQT, C50kQT and CQDs with different concentrations, respectively. (d-e) 293 T cells viability after treated by C30kQT/DNA and C50kQT/DNA complexes with different mass ratios, respectively. (f-g) 293 T cells viability after treated by RBCm-C30kQT/DNA, RBCm-C50kQT/DNA with different mass ratios, respectively. (h-j) HeLa cells viability after treated by C30kQT/DNA and C50kQT/DNA complexes with different concentrations, respectively. (k-l) HeLa cells viability after treated by C30kQT/DNA and C50kQT/DNA complexes with different mass ratios, respectively. (m-n) HeLa cells viability after treated by RBCm-C30kQT/DNA, RBCm-C50kQT/DNA with different mass ratios, respectively. (mean ± SD, n=3; $^{*}p \leq 0.05$, $^{**}p \leq 0.01$, $^{***}p \leq 0.001$, $^{****}p \leq 0.0001$).

pH = 7.4, and the maximum release efficiency at pH = 5.0 were 78.56 % and 73.40 %. The results showed that the release efficiency of carrier/DNA in weak acidic environment was high, and the microenvironment of tumor cells was weak acidic, so the carrier could achieve good release effect in tumor cells. As illustrated in Fig. 3**f-g**, the encapsulation rates of RBCm-C30kQT/DNA and RBCm-C50kQT/DNA showed an increasing trend with the increase of mass ratio and extrusion times. RBCmC30kQT and RBCm-C50kQT reached the maximum encapsulation rate of 75.62 % and 80.31 % at 2/1.5/1 and 3/1/1. In terms of extrusion frequency, The sealing efficiency of the cell membrane reached saturation after 10 times of extrusion, and 10 times of extrusion was the standard in the subsequent material preparation.

### *3.1.9. Stability analysis of RBCm-CQT/DNA complex in vitro*

As shown in Fig. 3**h**, the particle size of freshly prepared RBCm-CQT complex is around 200 nm. The particle size of RBCm-C30kQT/DNA

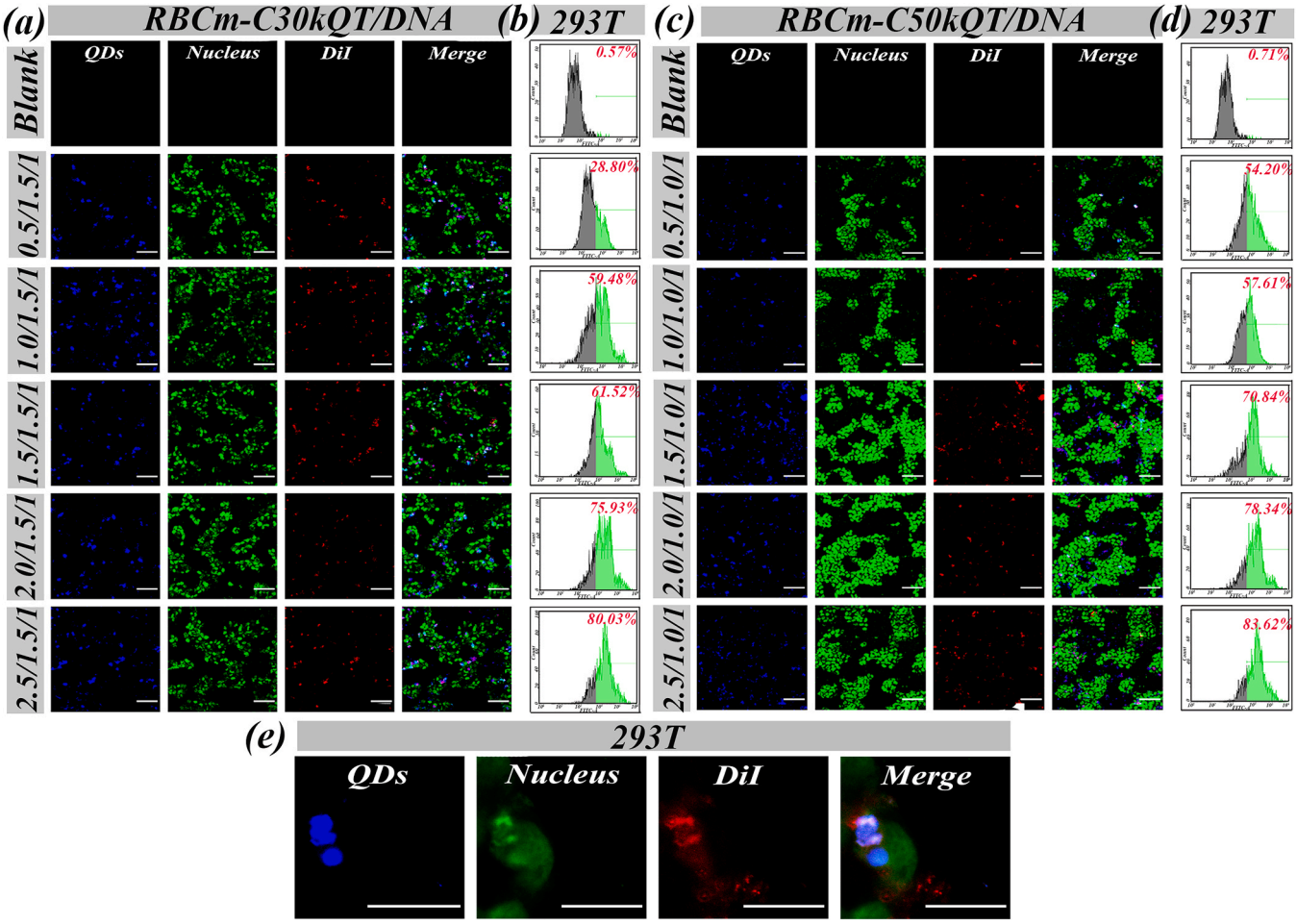


**Fig. 6.** Cellular uptake results of RBCm-C30kQT/DNA and RBCm-C50kQT/DNA complexes in 293 T cells. (a) Ingestion fluorescence images of RBCm-C30kQT/DNA complexes with different mass ratios in 293T cells (400×). Scale = 50μm. (b) The uptake efficiency of RBCm-C30kQT/DNA complex with different mass ratios in 293 T cells was measured by flow cytometry. (c) Ingestion fluorescence images of RBCm-C50kQT/DNA complexes with different mass ratios in 293T cells (400×). Scale = 50 μm; (d) The uptake efficiency of RBCm-C50kQT/DNA complex with different mass ratios in 293 T cells was determined by flow cytometry. (e) Locally amplified fluorescence images of RBCm-CQT/DNA complex 293T cells ingested. Scale = 10 μm.

complex remains unchanged from 0 to 14 days, but drastically increases to 817 nm after 21 days. This is because the complex encapsulated by the cell membrane is gradually released, causing the released nanoparticles to reaggregate and increase in size. According to Fig. 3**i**, the size of RBCm-C50kQT/DNA complex did not show significant changes from 0 to 21 days, but experienced a sudden increase in size after 28 days, reaching a final size of 825 nm. This could be due to an increase in the amount of cell membrane leading to enhanced stability of the membrane complex. In conclusion, the RBCm-C30kQT/DNA complex exhibits strong stability within 14 days. The RBCm-C50kQT/DNA complex, on the other hand, demonstrates strong stability within 21 days.

### *3.1.10. Agarose gel electrophoresis*

Whether the carrier can bind to DNA is the key to successfully transfer the therapeutic gene to the target cell [51]. Agarose gel electrophoresis was used to analyze the condensation ability of C30kQT and C50kQT with DNA. As shown in Fig. 4**a-b**, DNA showed a trend of gradual condensation with the increase of mass ratio, when the mass ratio of C30kQT and C50kQT was 1.5/1 and 1/1, they can completely condense with DNA, indicating that C30kQT and C50kQT have good binding ability to DNA. Compared with single Chitosan, the DNA condensation ability of the C30kQT and C50kQT have been significantly improved, which may be related to the particle size and Zata potential of the carrier.

The ability of C30kQT and C50kQT to protect and release DNA was verified by agarose gel electrophoresis, and the experimental results were shown in Fig. 4**c**. The absence of a band in group I indicated that DNA was completely bound to the carrier. After the complete binding of carrier and DNA in group II, Active Ingredient sodium was added to incubate at a certain temperature and time, and bright bands appeared in the gel channel, indicating the complete release of DNA. In group III, DNaseI was added after the carrier was completely bound to DNA, and there was no obvious band, indicating that DNA can stably exist in the hydrolase environment under the protection of the carrier. In group IV, the carrier was completely bound to DNA, and no obvious band was found, indi-cating that DNA was degraded by DNaseI in the case of sodium Active Ingredient replacement and loss of carrier protection. After the vector in group V was treated with inactivated DNaseI, obvious bands appeared after adding Active Ingredient sodium, indicating that inactivated DNaseI had no effect on DNA. In Fig. 4**d**, the results of DNA protection and release ability of RBCm-C30kQT/DNA and RBCm-C50kQT/DNA were consistent with C30kQT/DNA and C50kQT/DNA.

## *3.2. Cytotoxicity*

The safety of gene carrier in cells is one of the key factors to determine whether gene delivery system can be used in clinic. MTT assay was used to evaluate the toxicity of carrier/DNA complexes in 293 T and HeLa cells after co-incubation for 48 h. Fig. 5**a-c** and Fig. 5**h-j** displayed

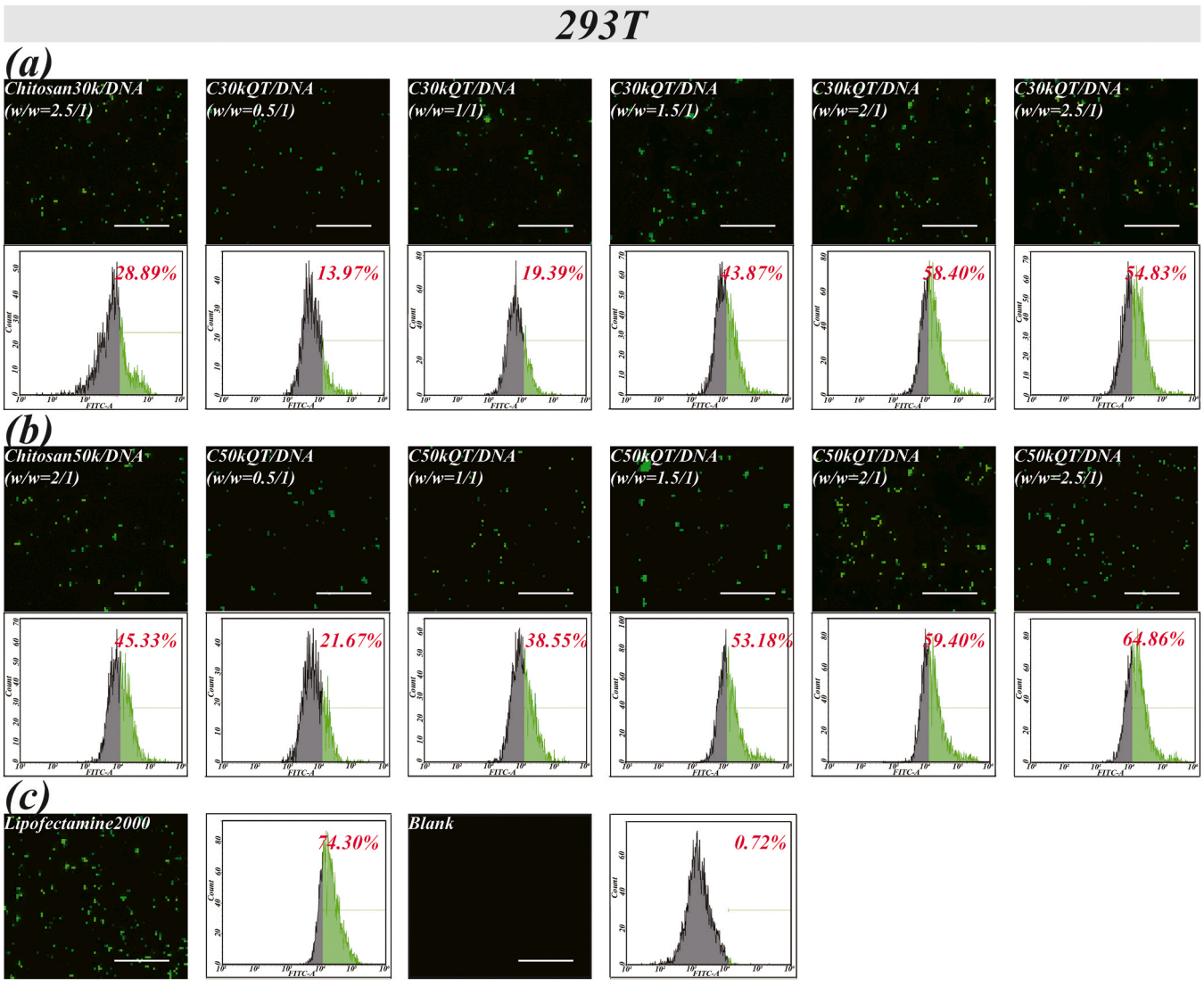


**Fig. 7.** Gene transfection results of QDs/DNA in 293 T cells. Transfection fluorescence images and flow cytometry analysis of transfection efficiency of pEGFP plasmid in cells treated by C30kQT/DNA(a), C50kQT/DNA(b), Lipofectamine 2000(c), scale bar = 1000 μm.

the effect of different concentrations of carriers on the activity of 293T cells and HeLa cells, compared with the single Chitosan30k and Chitosan50k, the cytotoxicity of C30kQT and C50kQT decreased significantly, and became more obvious with the increase of concentration. When the concentration reached 20 mg/L, the cell survival rate of C30kQT and C50kQT were higher than 70 %. Fig. 5**d-e** and Fig. 5**k-l** illustrated the effects of C30kQT/DNA and C50kQT/DNA with different mass ratios on the relative cell viability of 293 T cells and HeLa cells, with the increase of the mass ratio of C30kQT/DNA and C50kQT/DNA, the cell survival rates decreased significantly, indicating that C30kQT and C50kQT still have certain toxicity. By encapsulating the cell membrane of C30kQT and C50kQT, and then investigating the cytotoxicity, the results were shown in Fig. 5**f-g** and Fig. 5**m-n**. The cytotoxicity was negatively correlated with the quality of cell membrane. With the increase of mass ratio, the cytotoxicity of RBCm-C30kQT/DNA and RBCm-C50kQT/DNA in 293T cells and HeLa cells decreased accordingly. When the maximum mass ratio was 4/1.5/1, the cell survival rates of RBCm-C30kQT/DNA in 293 T cells and HeLa cells were 86.2 % and 92.95 %. When the maximum mass ratio of RBCm-C50kQT/DNA was 4/1/1, the cell survival rates of 293T cells and HeLa cells were 88.53 % and 90.57 %. The results showed that cell membrane encapsulation could effectively reduce cytotoxicity. We also investigated the toxicity of the carrier /DNA complex to 293T cells and HeLa cells after 72 h co-incubation (Fig. S1). The overall trend was the same as that of the cell toxicity after 48 h co-incubation, and the relative cell viability decreased somewhat but not significantly, which further proved that the carrier /DNA had good safety.

### 3.3. *In vitro cell uptake*

The uptake efficiency of C30kQT/DNA and C50kQT/DNA in 293 T cells and HeLa cells were investigated by fluorescence microscopy and flow cytometry. As shown in Fig. S2a, Fig. S2c, Fig. S3a and Fig. S3c, C30kQT/DNA and C50kQT/DNA successfully entered 293 T cells and HeLa cells under the fluorescence microscope. The uptake efficiency of C30kQT/DNA and C50kQT/DNA in 293 T cells increased with the increase of mass ratio, reaching 65.77 % and 73.27 % when the mass ratio was 2.5/1 (Fig. S2b and Fig. S2d). The uptake efficiency of C30kQT/DNA and C50kQT/DNA in HeLa cells were shown in Fig. S3b and Fig. S3d, and the uptake efficiency reached 60.48 % and 80.77 % at a mass ratio of 2.5/1. The uptake efficiency of C50kQT/DNA in 293 T cells and HeLa cells was significantly higher than that of C30kQT/DNA, indicating that the complex made of high molecular weight chitosan was more easily taken up by cells. As illustrated in Fig. 6**a** and Fig. 6**c**, RBCm-

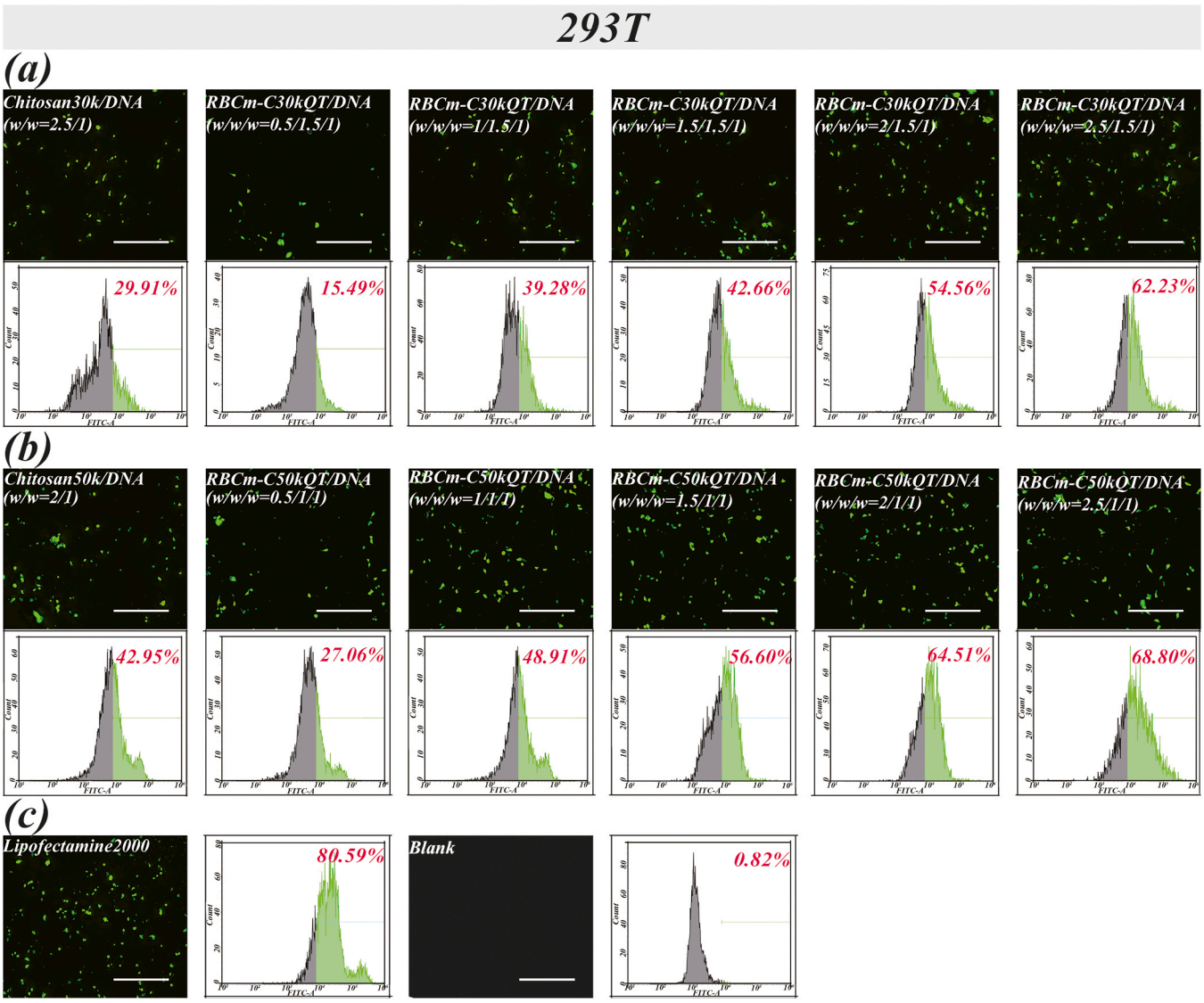


**Fig. 8.** Gene transfection results of RBCm-CQT/DNA complex in 293 T cells. Transfection fluorescence images and flow cytometry analysis of transfection efficiency of pEGFP plasmid in cells treated by RBCm-C30kQT/DNA(a), RBCm-C50kQT/DNA(b), Lipofectamine 2000(c), scale bar = 1000 μm.

C30kQT/DNA and RBCm-C50kQT/DNA could be taken up by 293 T cells in different degrees, the blue part in the figure (C30kQT, C50kQT) and the green part (nucleus) coincided to a certain extent, indicating that the sample could be successfully taken up by 293T cells, and its maximum intake efficiency was 80.03 % and 83.62 % (Fig. 6**b** and Fig. 6**d**). Fig. S4a and Fig. S4c show that RBCm-C30kQT/DNA and RBCm-C50kQT/DNA can be successfully taken into HeLa cells, and their intake efficiency reached 73.27 % and 77.45 % (Fig. S4b and Fig. S4d). The above results indicate that cell membrane encapsulation can effectively promote the uptake of the complex, making it have higher cellular uptake efficiency.

### *3.4. In vitro gene transfection*

Fluorescence microscopy and flow cytometry were used to evaluate the gene transfection efficiency of C30kQT/DNA and C50kQT/DNA in 293T and HeLa cells, the results were displayed in Fig. 7 and Fig. S5. The expression of green fluorescent protein was observed in both 293 T and HeLa cell lines, and the transfection efficiency of the samples gradually increased with the increase of DNA binding ratio. The maximum transfection efficiency of C30kQT/DNA in 293 T cells was 58.40 % at a mass ratio of 2/1 and C50kQT/DNA in 293 T cells was 64.86 % at a mass ratio of 2.5/1, which were higher than those of chitosan/DNA at the same mass ratio (28.89 % and 45.33 %). The transfection of C30kQT/DNA and C50kQT/DNA in HeLa cells was similar to that in 293 T cells, and the transfection efficiency reached 35.83 % and 40.46 % at the mass ratio of 2.5/1 and 2.5/1, respectively. The above results showed that the composite quantum dots were contribute to improve the transfection efficiency of the carriers. The transfection efficiencies of RBCm-C30kQT/DNA and RBCm-C50kQT/DNA in 293 T and HeLa cells were illustrated in Fig. 8 and Fig. S6. In 293T cells, Both RBCm-C30kQT/DNA and RBCm-C50kQT/DNA showed high transfection efficiency, the transfection efficiency of RBCm-C30kQT/DNA at the mass ratio of 2.5/1.5/1 was 62.23 %, the transfection efficiency of RBCm-C50kQT/DNA at the mass ratio of 2.5/1/1 was 68.80 %, which was higher than that of CQT/DNA. In HeLa cells, the transfection efficiency of RBCm-C30kQT/DNA at the mass ratio of 2.5/1.5/1 was 41.63 %, the transfection efficiency of RBCm-C50kQT/DNA at the mass ratio of 2.5/1/1 was 45.47 %. The transfection efficiency of RBCm-C50kQT/DNA was higher than RBCm-C30kQT/DNA in both 293 T cells and HeLa cells, indicating that RBCm-C50kQT has more potential as a gene carrier.

## 4. Conclusion

In summary, we constructed a tracer bionic gene delivery carrier based on chitosan for safe and efficient gene delivery. Carbon quantum dots were prepared by a simple hydrothermal method and connected to chitosan under the action of TPP to obtain C50kQT. In weakly acidic environments, the gene release efficiency of C50kQT/DNA is higher, which reached 78.56 %, indicating that the carrier can achieve good release effect in tumor cells. The toxicity of the carrier was reduced and biocompatibility was improved through cell membrane encapsulation. RBCm-C50kQT can effectively carry DNA and protect it from degradation, ensuring successful release to improve gene delivery efficiency. In addition, RBCm-C50kQT/DNA not only maintains good fluorescence tracking characteristics, but also reduces cell toxicity and improves uptake and transfection efficiency. The *in vitro* transfection experiments of 293 T and HeLa cells showed that the maximum transfection efficiency of RBCm-C50kQT/DNA reached 68.80 % and 45.47 %, respectively. Therefore, chitosan based traceable biomimetic gene delivery carriers have potential clinical application prospects, which can improve gene delivery efficiency, reduce cell toxicity, and provide a simple and effective strategy for the preparation of efficient gene delivery carriers.

## CRediT authorship contribution statement

**Jiayu He:** Data curation, Formal analysis, Methodology, Resources, Validation, Conceptualization, Writing – review & editing. **Peng Hu:** Data curation, Formal analysis. **Mingjie Wang:** Investigation, Validation. **Guowei Qi:** Methodology. **Haoxiang Huang:** Visualization. **Dong Zeng:** Conceptualization. **Jintao Guan:** Visualization. **Peiwen Lv:** Resources. **Liang Liu:** Conceptualization, Visualization, Writing – review & editing, Funding acquisition.

## Declaration of Competing Interest

We declare that we have no financial and personal relationships with other people or organizations that can inappropriately influence our work, there is no professional or other personal interest of any nature or kind in any product, service and/or company that could be construed as influencing the position presented in, or the review of, the manuscript entitled, "*Utilization of chitosan nanocomposites loaded with quantum dots enables efficient and traceable DNA delivery*".

## Data Availability

Data will be made available on request.

## Acknowledgements

This research was funded by the National Natural Science Foundation of CN (21602166), the Natural Science Foundation of Hubei Province (2020CFB760), and the Research and Innovation Initiatives of WHPU (2021Y11). The authors also acknowledge the support of Shiyanjia Lab (www.shiyanjia.com) for the structure (such as TEM) measurement.

### *Conflict of interest*

The authors declare no conflict of interest.

## Appendix A. Supporting information

Supplementary data associated with this article can be found in the online version at doi:10.1016/j.colsurfb.2024.114221.

## References

[1] M.H. Butt, M. Zaman, A. Ahmad, R. Khan, T.H. Mallhi, M.M. Hasan, Y.H. Khan, S. Hafeez, E.E. Massoud, M.H. Rahman, S. Cavalu, Appraisal for the potential of viral and nonviral vectors in gene therapy: a review, Genes 13 (2022) 27.
[2] C. Wang, C. Pan, H. Yong, F. Wang, T. Bo, Y. Zhao, B. Ma, W. He, M. Li, Emerging non-viral vectors for gene delivery, J. Nanobiotechnol 21 (2023) 272.
[3] S. Ren, M. Wang, C. Wang, Y. Wang, C. Sun, Z. Zeng, H. Cui, X. Zhao, Application of non-viral vectors in drug delivery and gene therapy, Polym. (Basel) 13 (2021).
[4] S. Karthik, S. Mohan, I. Magesh, A. Bharathy, R. Kolipaka, S. Ganesamoorthi, K. Sathiya, A. Shanmugavadivu, R. Gurunathan, N. Selvamurugan, Chitosan nanocarriers for non-coding RNA therapeutics: a review, Int J. Biol. Macromol. 263 (2024) 130361.
[5] A.S. Soubhagya, M. Prabaharan, Chitosan-Based Theranostics for Cancer Therapy, in: R. Jayakumar, M. Prabaharan (Eds.), Chitosan for Biomaterials Iv: Biomedical Applications, Springer International Publishing Ag, Cham, 2021, pp. 271–292.
[6] F.D. Moghaddam, E.N. Zare, M. Hassanpour, F.R. Bertani, A. Serajian, S.F. Ziaei, A. C. Paiva-Santos, R.E. Neisiany, P. Makvandi, S. Iravani, Y. Xu, Chitosan-based nanosystems for cancer diagnosis and therapy: Stimuli-responsive, immune response, and clinical studies, Carbohydr. Polym. 330 (2024) 121839.
[7] S. Sargazi, B. Siddiqui, M. Qindeel, A. Rahdar, M. Bilal, R. Behzadmehr, S. Mirinejad, S. Pandey, Chitosan nanocarriers for microRNA delivery and detection: A preliminary review with emphasis on cancer, Carbohydr. Polym. 290 (2022) 119489.
[8] R. Nair, P. Paul, I. Maji, U. Gupta, S. Mahajan, M. Aalhate, S.K. Guru, P.K. Singh, Exploring the current landscape of chitosan-based hybrid nanoplatforms as cancer theragnostic, Carbohydr. Polym. 326 (2024) 121644.
[9] F. Yu, Y. Zhu, X. Shang, H. Yuan, F. Hu, Rationally-designed chitosan-based polymeric nanomaterials according to intrinsic characteristics for cancer therapy and theranostics: a review, Curr. Med Chem. 30 (2023) 1368–1385.
[10] M. Minoshima, S.I. Reja, R. Hashimoto, K. Iijima, K. Kikuchi, Hybrid small-molecule/protein fluorescent probes, Chem. Rev. 124 (2024) 6198–6270.
[11] E.G. Ehrhorn, P. Lovell, D. Svechkarev, S. Romanova, A.M. Mohs, Optimizing the performance of silica nanoparticles functionalized with a near-infrared fluorescent dye for bioimaging applications, Nanotechnology 35 (2024).
[12] D.J. Si, Q.L. Li, Y.F. Bao, J.Y. Zhang, L. Wang, Fluorogenic and cell-permeable rhodamine dyes for high-contrast live-cell protein labeling in bioimaging and biosensing, Angew. Chem. -Int. Ed. 62 (2023) 14.
[13] A. Hlaváček, Z. Farka, M.J. Mickert, U. Kostiv, J.C. Brandmeier, D. Horák, P. Skládal, F. Foret, H.H. Gorris, Bioconjugates of photon-upconversion nanoparticles for cancer biomarker detection and imaging, Nat. Protoc. 17 (2022) 1028–1072.
[14] X. Kang, M. Zhu, Tailoring the photoluminescence of atomically precise nanoclusters, Chem. Soc. Rev. 48 (2019) 2422–2457.
[15] S. Harchouni, B. Field, B. Menand, AC-202, a highly effective fluorophore for the visualization of lipid droplets in green algae and diatoms, Biotechnol. Biofuels 11 (2018) 120.
[16] N. Le, M. Zhang, K. Kim, Quantum dots and their interaction with biological systems, Int J. Mol. Sci. 23 (2022).
[17] P. Chakraborty, S.S. Das, A. Dey, A. Chakraborty, C. Bhattacharyya, R. Kandimalla, B. Mukherjee, A.V. Gopalakrishnan, S.K. Singh, S. Kant, P. Nand, S. Ojha, P. Kumar, N.K. Jha, S.K. Jha, S. Dewanjee, Quantum dots: the cutting-edge nanotheranostics in brain cancer management, J. Control Release 350 (2022) 698–715.
[18] M.A. Jahangir, S.J. Gilani, A. Muheem, M. Jafar, M. Aslam, M.T. Ansari, M. A. Barkat, Quantum dots: next generation of smart nano-systems, Pharm. Nanotechnol. 7 (2019) 234–245.
[19] Q. Xu, J. Gao, S. Wang, Y. Wang, D. Liu, J. Wang, Quantum dots in cell imaging and their safety issues, J. Mater. Chem. B 9 (2021) 5765–5779.
[20] W.X. Wang, Z. Liu, X.L. Lan, Quantum dot-based simultaneous multicolor imaging, Mol. Imaging Biol. 22 (2020) 820–831.
[21] H. Lu, W. Li, H. Dong, M. Wei, Graphene quantum dots for optical bioimaging, Small 15 (2019) e1902136.
[22] I. Mahlooji, J. Javidi, S. Dadashzadeh, Pharmacokinetics, tissue distribution and peritoneal retention of Ag2S quantum dots following intraperitoneal administration to mice, J. Pharm. Pharm. 73 (2021) 1599–1608.
[23] Y. Sun, S. Wang, M. Wang, M. Wang, C. Liu, L. Liu, Development of a biomimetic DNA delivery system by encapsulating polyethyleneimine functionalized silicon quantum dots with cell membranes, Colloids Surf. B Biointerfaces 230 (2023) 113507.
[24] J. Sobhanan, A. Anas, V. Biju, Nanomaterials for fluorescence and multimodal bioimaging, Chem. Rec. 23 (2023) e202200253.
[25] A. Hamidu, W.G. Pitt, G.A. Husseini, Recent breakthroughs in using quantum dots for cancer imaging and drug delivery purposes, Nanomater. (Basel) 13 (2023).
[26] L. Dirheimer, T. Pons, F. Marchal, L. Bezdetnaya, Quantum dots mediated imaging and phototherapy in cancer spheroid models: state of the art and perspectives, Pharmaceutics (14 () (2022).
[27] T.Y. Shen, P.Y. Jia, D.S. Chen, L.N. Wang, Hydrothermal synthesis of N-doped carbon quantum dots and their application in ion-detection and cell-imaging, Spectrochim. Acta A Mol. Biomol. Spectrosc. 248 (2021) 119282.
[28] L. Upadhyaya, J. Singh, V. Agarwal, A.C. Pandey, S.P. Verma, P. Das, R.P. Tewari, Efficient water soluble nanostructured ZnO grafted O-carboxymethyl chitosan/curcumin-nanocomposite for cancer therapy, Process Biochem 50 (2015) 678–688.
[29] S. Ghosh, K. Ghosal, S.A. Mohammad, K. Sarkar, Dendrimer functionalized carbon quantum dot for selective detection of breast cancer and gene therapy, Chem. Eng. J. 373 (2019) 468–484.

[30] J. Sobhanan, J.V. Rival, A. Anas, E. Sidharth Shibu, Y. Takano, V. Biju, Luminescent quantum dots: Synthesis, optical properties, bioimaging and toxicity, Adv. Drug Deliv. Rev. 197 (2023) 114830.
[31] X.X. Yao, R.E. Lewis, C.L. Haynes, Synthesis processes, photoluminescence mechanism, and the toxicity of amorphous or polymeric carbon dots, Acc. Chem. Res. 10 (2022).
[32] J. Janus, M. Radwan-Pragłowska, D. Piątkowski, Bogdał, Facile synthesis of surface-modified carbon quantum dots (CQDs) for biosensing and bioimaging, Mater. (Basel) 13 (2020).
[33] S. Zhang, X. Zhang, H. Gao, X. Zhang, L. Sun, Y. Huang, J. Zhang, B. Ding, Cell membrane-coated biomimetic nanoparticles in cancer treatment, Pharmaceutics 16 (2024).
[34] H. Liu, Y.Y. Su, X.C. Jiang, J.Q. Gao, Cell membrane-coated nanoparticles: a novel multifunctional biomimetic drug delivery system, Drug Deliv. Transl. Res 13 (2023) 716–737.
[35] J. Zhao, J. Ruan, G. Lv, Q. Shan, Z. Fan, H. Wang, Y. Du, L. Ling, Cell membrane-based biomimetic nanosystems for advanced drug delivery in cancer therapy: a comprehensive review, Colloids Surf. B Biointerfaces 215 (2022) 112503.
[36] Y. Zeng, S. Li, S. Zhang, L. Wang, H. Yuan, F. Hu, Cell membrane coated-nanoparticles for cancer immunotherapy, Acta Pharm. Sin. B 12 (2022) 3233–3254.
[37] Y. Jiang, N. Krishnan, J. Zhou, S. Chekuri, X. Wei, A.V. Kroll, C.L. Yu, Y. Duan, W. Gao, R.H. Fang, L. Zhang, Engineered cell-membrane-coated nanoparticles directly present tumor antigens to promote anticancer immunity, Adv. Mater. 32 (2020) e2001808.
[38] X. Wang, Z. Xia, H. Wang, D. Wang, T. Sun, E. Hossain, X. Pang, Y. Liu, Cell-membrane-coated nanoparticles for the fight against pathogenic bacteria, toxins, and inflammatory cytokines associated with sepsis, Theranostics 13 (2023) 3224–3244.
[39] X. Huang, H. Guo, L. Wang, Z. Zhang, W. Zhang, Biomimetic cell membrane-coated nanocarriers for targeted siRNA delivery in cancer therapy, Drug Discov. Today 28 (2023) 103514.
[40] D.X. Zhang, G.D. Wang, N.Y. Ma, Z.Y. Yuan, Y.Q. Dong, X. Huang, H.S. Qiao, K. Ren, Biomedical applications of cell membrane-based biomimetic nano-delivery system, Adv. Ther. 7 (2024) 23.
[41] B.D. Zheng, M.T. Xiao, Red blood cell membrane nanoparticles for tumor phototherapy, Colloid Surf. B-Biointerfaces 220 (2022) 17.
[42] M.Y. Wang, Y.L. Sun, M.J. Wang, Z.J. Yang, Y. Shi, D. Zeng, L. Liu, Enhancing the safety and effectiveness of polyethylenimine gene delivery through cell membrane encapsulation, J. Drug Deliv. Sci. Technol. 92 (2024) 14.
[43] X. Liang, H. Li, A. Zhang, X. Tian, H. Guo, H. Zhang, J. Yang, Y. Zeng, Red blood cell biomimetic nanoparticle with anti-inflammatory, anti-oxidative and hypolipidemia effect ameliorated atherosclerosis therapy, Nanomedicine 41 (2022) 102519.
[44] R.J. Byers, E.R. Hitchman, Quantum dots brighten biological imaging, Prog. Histochem Cytochem 45 (2011) 201–237.
[45] H. Jafari, H. Namazi, G.R. Mahdavinia, pH-sensitive biocompatible chitosan/sepiolite-based cross-linked citric acid magnetic nanocarrier for efficient Active Ingredient release, Int. J. Biol. Macromol. 242 (2023) 124739.
[46] J. Yang, A. Duan, L. Shen, Q. Liu, F. Wang, Y. Liu, Preparation and application of curcumin loaded with citric acid crosslinked chitosan-gelatin hydrogels, Int. J. Biol. Macromol. 264 (2024) 130801.
[47] M. Pooresmaeil, H. Namazi, Hyaluronic acid functionalized citric acid dendrimer/UiO-66-COOH as a stable and biocompatible platform for Active Ingredient delivery, Int J. Biol. Macromol. 268 (2024) 131590.
[48] Y. Xiao, Z. Tang, X. Huang, W. Chen, J. Zhou, H. Liu, C. Liu, N. Kong, W. Tao, Emerging mRNA technologies: delivery strategies and biomedical applications, Chem. Soc. Rev. 51 (2022) 3828–3845.
[49] M. Wu, H. Guo, L. Liu, Y. Liu, L. Xie, Size-dependent cellular uptake and localization profiles of silver nanoparticles, Int J. Nanomed. 14 (2019) 4247–4259.
[50] H.J. Je, E.S. Kim, J.S. Lee, H.G. Lee, Release properties and cellular uptake in Caco-2 cells of size-controlled chitosan nanoparticles, J. Agric. Food Chem. 65 (2017) 10899–10906.
[51] H. Zu, D. Gao, Non-viral vectors in gene therapy: recent development, challenges, and prospects, Aaps J. 23 (2021) 78.